# Dependency of sliding friction for two-dimensional systems on electronegativity

Jianjun Wang , 1,2,4 Avinash Tiwari, Jie Gao, Yang Huang , Yu Jia , 2,3,\* and Bo N. J. Persson 

1 Zhengzhou Key Laboratory of Low-Dimensional Quantum Materials and Devices, and College of Science,

Zhongyuan University of Technology, Zhengzhou, Henan 450007, China

2 Key Laboratory for Special Functional Materials of Ministry of Education, and School of Materials Science and Engineering,

Henan University, Kaifeng, Henan 475004, China

3 International Laboratory for Quantum Functional Materials of Henan, and School of Physics,

Zhengzhou University, Zhengzhou, Henan 450001, China

4 PGI-1, FZ-Juelich, Germany, EU

(Received 16 June 2020; revised 5 January 2022; accepted 13 April 2022; published 27 April 2022)

We study the role of electronegativity in sliding friction for five different two-dimensional (2D) monolayer systems using *ab initio* calculations within density functional theory with van der Waals corrections. We show that the friction depends strongly on the involved atoms' electronegativity difference. All the studied systems exhibit almost the same magnitude of the friction force when sliding along the nonpolar path, independent of the material and the surface structures. In contrast, for sliding friction along a polar path, the friction force obeys a universal linear scaling law where the friction force is proportional to the electronegativity difference of its constituent atoms. We show that atomic dipoles in the 2D monolayers, induced by the electronegativity difference, enhance the corrugation of the charge distribution and increase the sliding barriers accordingly. Our studies reveal that electronegativity plays an important role in the friction of low-dimensional systems, and provides a strategy for designing nanoscale devices.

### DOI: 10.1103/PhysRevB.105.165431

# I. INTRODUCTION

Understanding the origin of atom-scale friction, and controlling it when designing nanotechnological devices, pose a major challenge due to the intricate interfacial interaction [1,2]. Two-dimensional (2D) layered materials, such as graphene, hexagonal boron nitride (*h*-BN), and hexagonal molybdenum disulfide (MoS<sub>2</sub>), due to their strong intralayer chemical bonding compared with the weak interlayer physical adsorption interaction, can serve as solid lubricants to minimize friction and wear in many applications [3–5]. Moreover, 2D layered structures often have novel electronic properties widely researched in the literature, which can further our understanding of their tribological behavior [6–9].

Friction is ultimately governed by the atomistic interactions determined by quantum mechanics [1,2,9]. Several studies have demonstrated that electronic structure and charge distribution are closely related to the friction behavior of low-dimensional systems [5,7–10]. The electronegativity difference among the constituent atoms is closely related to the friction in low-dimensional materials [11–15]. Experiments have shown that the sliding friction in an insulating multiwall boron nitride nanotube (BNNT) is orders of magnitude stronger than that of a semimetallic carbon nanotube, which was attributed to an increased potential barrier caused by the charge localization induced by the electronegativity difference

between the boron and nitrogen atoms in BNNT [11]. This localization effect increases the corrugation amplitude of the interfacial potential. Similarly, *ab initio* molecular dynamics simulation showed that the coefficient of friction (COF) of liquid water sliding on h-BN is about three times larger than that of graphene, which was ascribed to the greater corrugation of the energy landscape of h-BN [12].

From density functional theory (DFT) calculations, it was found that the van der Waals (vdW) interaction determines the interlayer binding, and the electrostatic interaction influences the sliding barrier for *h*-BN sliding on *h*-BN [13]. Hod speculated that a highly anisotropic interfacial friction should exist for the *h*-BN bilayer [14]. Gao and Tkatchenko showed that the contributions of electrostatic and dispersive interactions to the sliding energy profile are different in bilayer graphene and *h*-BN [15]. These results presented above confirm that polarity plays an important role in friction for low-dimensional systems. However, few studies showing a clear connection between polarity and friction properties have been established.

In this study, *ab initio* calculations were carried out to investigate the role of electronegativity on friction in 2D systems. We find that when two monolayers slide relative to each other, the atom electronegativity difference along the sliding path strongly influences the interfacial friction properties; that is, the friction scales linearly with the electronegativity difference in the sliding path.

Here we note that the potential barrier which the system must overcome to move along the sliding (reaction) path, where the total (adiabatic) energy is minimal, is very relevant for sliding friction. For slow motion uphill along this

<sup>\*</sup>jiayu@zzu.edu.cn

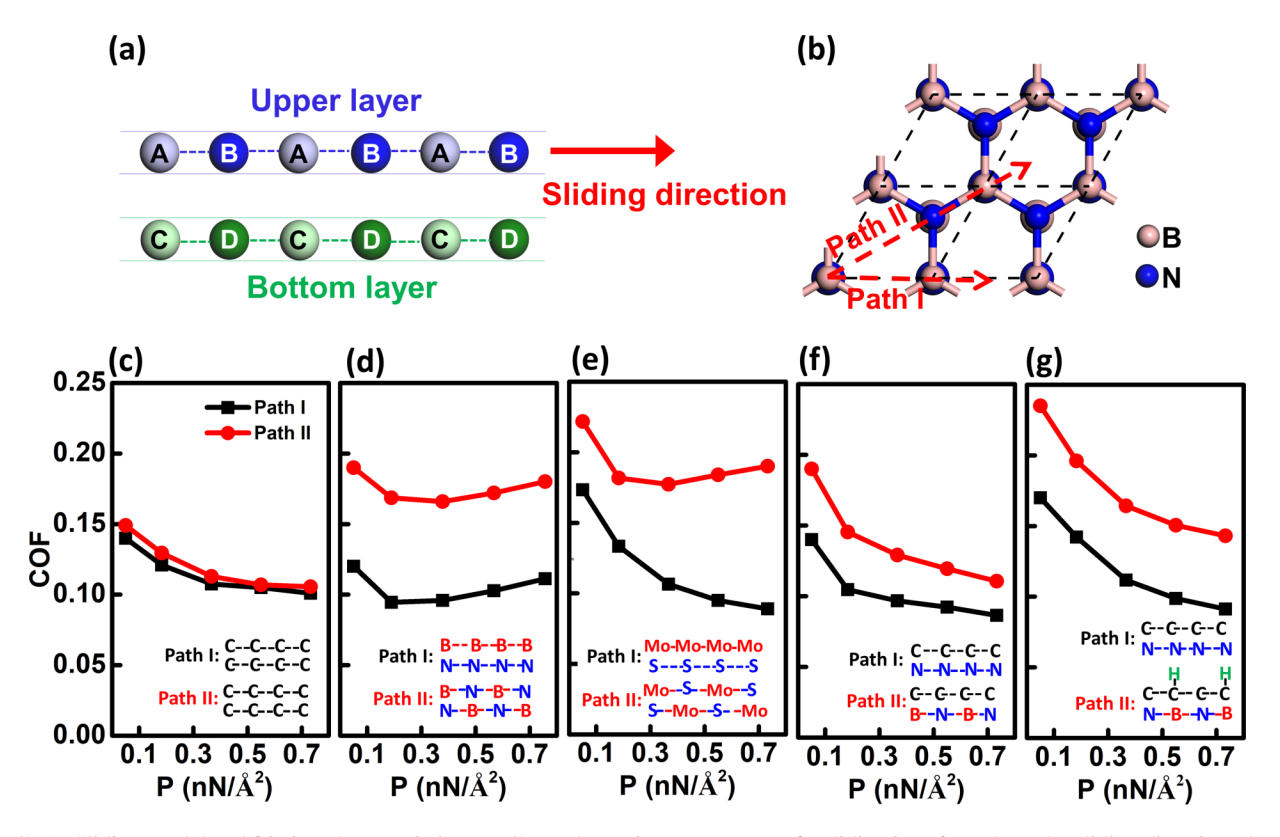


FIG. 1. Sliding model and friction characteristics. (a) General atomic arrangement of a sliding interface along the sliding direction. (b) Two sliding paths illustrated by h-BN/h-BN system with AA′ stacking as an example. Coefficient of friction as a function of normal pressure along polar and nonpolar paths for (c) graphene/graphene, (d) h-BN/h-BN, (e) MoS $_2$ /MoS $_2$ , (f) graphene/h-BN, and (g) H-graphene/h-BN systems.

path the system must climb an energetic barrier which determines the so-called static friction force, at least at low temperature where thermal activation is unimportant. In reality there are many complications such as impurity molecules, surface roughness, and long-range elasticity effects which could complicate the picture, but these are almost impossible to include in a fully quantum mechanical model study, and would vary, anyway, from one case to another. If one assumes that all the potential energy gained on climbing to the top of the potential barrier is lost as vibrational energy during the downhill motion then the calculations presented below would also give an estimation of the kinetic friction. We note that there are very few (if any) studies where the full dynamics of the energy loss process (emission of phonons, and excitation of low-energy electron-hole pairs for conducting materials) is included in the analysis and fewer still involving quantum mechanical calculations. Thus, to correctly account for these energy loss processes requires huge system size to obtain a near continuum of energy levels and irreversibility in the energy transfer process. Still the nature of the energy transfer process is irrelevant for the kinetic friction force if one assumes that the system spends enough time close to the bottom of the potential wells to (nearly) fully thermalize.

#### II. METHODS AND CALCULATIONS

The Vienna Ab Initio Simulation Package (VASP) code, based on the projector augmented-wave (PAW) method,

was employed in the calculations [16–18]. The exchange-correlation interactions were treated with the generalized gradient approximation (GGA) of Perdew, Burke, and Ernzerhof (PBE) [19], with a vdW correction determined by the many-body dispersion (MBD) method [20]. An energy cutoff of 600 eV and  $21 \times 21 \times 1$  Monkhorst-Pack grids were selected for the 2D irreducible Brillouin-zone integration [21]. The convergence thresholds for total energy and Hellmann-Feynman forces are  $10^{-5}$  eV and 0.01 eV/Å, respectively. A vacuum space of at least 20 Å was set to avoid intercell interactions. In the process of making the calculations, the in-plane lattice constants of the bilayer structures were kept fixed.

In order to study the influence of polarity on friction, we first discuss the sliding path's polarity character. Figure 1(a) shows a schematic diagram of the sliding interface between two monolayers. The atoms A, B from the upper layer, and C, D from the bottom layer are arranged alternating along the sliding direction. We define the sliding system's total polarity along the sliding direction as the sum of the polarity of each single layer in that direction, which is decided by the electronegativity differences between A, B atoms, and C, D atoms. Here, the h-BN bilayer is chosen as an example to illustrate the polarity differences in different paths [see Fig. 1(b)]. The most stable AA' stacking (where B eclipsed N atoms) was chosen as an initial structure [13,14,22], and two highly symmetric directions were chosen as sliding paths. From the Fig. 1(b), we can see that there is only one kind of B (N) atom in the upper (bottom) layer along path I, and so the

polarity is zero along this direction. However, B and N atoms are alternately arranged in the upper and the bottom layers along path II, which gives rise to in-plane dipoles in both layers. Therefore, we denote path I as nonpolar and path II as polar paths. The static friction is determined by the magnitude of the potential barrier along the sliding path [23–25]. Thus, depending on the sliding paths, different static friction values could be obtained [9,26,27]. In the *h*-BN bilayer case, the sliding paths with maximum polarity, and with nonpolarity, are chosen to understand the relationship between electronegativity and friction.

Along each sliding path, 13 stackings were selected for each sliding period to calculate friction characters. For each stacking, the binding energy of the bilayer system is calculated by  $E_{be} = E_{12} - E_1 - E_2$ , where  $E_{12}$  is the total energy of the bilayer and  $E_1$ ,  $E_2$  are energies of the isolated single layers of the bilayer, and then the normal load  $F_N$  can be exerted on the bilayer system by setting its interlayer distances z according to the function  $F_N = -\partial E_{be}(z)/\partial z$ . Thus, the potential energy at the position x under pressure  $F_N$  is  $V(x, F_N) = E_{be}[x, z(x, F_N)] + F_N z(x, F_N)$ . We define average friction force as  $\langle F_f \rangle = [V_{\text{max}}(F_N) - V_{\text{min}}(F_N)]/\Delta x$ , where  $V_{\text{max}}(F_N)$  and  $V_{\text{min}}(F_N)$  are the maximum and minimum of potential energy along one sliding path, and  $\Delta x$  is the distance between them. The shear stress  $\tau = \langle F_f \rangle / A$  is the average friction force divided by the surface area A [28].

### III. RESULTS AND DISCUSSION

The optimized lattice parameters of graphene, *h*-BN, and MoS<sub>2</sub> are 2.47, 2.51, and 3.18 Å, respectively. Using these lattice parameters, the most stable bilayer stacking was obtained (see Tables S1 and S2 in the Supplemental Material [29]), and is supported by other studies [13–15,30–37]. Two sheets of the 2D monolayer were moved relative to each other along paths I and II to simulate the sliding process (see Figs. 1(a) and 1(b) and Fig. S1 in the Supplemental Material [29]).

In order to reflect the changes of the friction potential barrier with the application of loads, we use a similar classical coefficient of friction  $\mu$ , calculated by  $\mu = \langle F_f \rangle / F_N$ , to characterize the magnitude of friction on different paths, where the friction is determined by the difference of the maximum and minimum potential energy in the unit cell along a sliding path [8,28]. It also should be noted that the friction calculated is the static (or break-loose) friction force. However, if it is assumed that all the energy needed to reach the top of the energy barrier is dissipated before climbing the next barrier, the presented calculations also give information about the kinetic friction [38]. The COF is calculated as a function of the load, and is shown in Figs. 1(c)-1(g). For the identical pristine bilayers, the COFs fall in a range of 0.07-0.2, which agrees with earlier studies [4,8]. Among these systems, the nonpolar graphene/graphene system [Fig. 1(c)] exhibits isotropic friction behavior. However, in the polar h-BN/h-BN [Fig. 1(d)] and MoS<sub>2</sub>/MoS<sub>2</sub> [Fig. 1(e)] systems, the COF exhibits anisotropic behavior, in which the COF along the polar path II is almost two times larger than for the nonpolar path.

We have examined the effect of electronegativity on the frictional properties for different sliding paths and found that

the friction along a polar path is larger than along a nonpolar path (see Fig. S2 in the Supplemental Material [29]). Even for the minimum potential barrier path (a zigzag path), the friction of polar bilayer h-BN is still larger than that for the nonpolar graphene system (see Fig. S3 in the Supplemental Material [29]). We also studied the variation of the COF on these two paths with the application of different loads. It is found that such effect of electronegativity is still significant when the load reaches an extremely large value,  $0.7 \, \text{nN/Å}^2$ , showing that polarity plays an important part in the friction between two polar planes.

We next investigated the friction between polar and non-polar sheets using the interface of graphene sliding on *h*-BN (graphene/*h*-BN; see Fig. S1(b) in the Supplemental Material [29]). The computational model was simplified by enlarging the lattice constant of graphene to be equal to that of *h*-BN so that a commensurate interface could be formed. Although the upper layer is nonpolar, path II is still polar due to dipoles in the bottom layer along the sliding path [Fig. 1(f)]. Like the polar/polar interface, the COF in the nonpolar/polar system is also anisotropic. Again, it indicates that the polarity still has a significant influence on friction even if dipoles exist only in one layer of the sliding interface.

Based on the graphene/h-BN system, we further consider the friction modulation by tuning the polarity of graphene. For this purpose, we induced polarity in the graphene lattice by single-side half hydrogenation (H-graphene, Fig. S1(c) in the Supplemental Material [29]). The covalent C-C bond in graphene turns into a partially ionic bond in H-graphene, with the charge transfer of 0.35 e. The COF between H-graphene and h-BN (H-graphene/h-BN) was calculated and is shown in Fig. 1(g). It is apparent that the COF along polar path II is larger than that of the nonpolar path I. More importantly, the H-graphene/h-BN system has a larger COF than that of the graphene/h-BN and is consistent with the increase of the polarity induced by hydrogenation passivation. These calculations provide insight on how to modify friction by surface modification.

The variation of the binding energy as a function of the relative lateral position of the two surfaces in contact is denoted as the potential energy surface (PES) [39]. The corrugation of the PES determines the intrinsic resistance to sliding and indicates the maximum energy that can be dissipated during frictional processes. In this calculation, the atoms at each stacking are allowed to fully relax along the vertical direction and so we construct an actual PES at zero pressure. To do this, three typical systems are chosen to represent the nonpolar/nonpolar, nonpolar/polar, and polar/polar cases, namely, graphene/graphene, graphene/h-BN, and h-BN/h-BN, respectively. The calculated PESs are shown in Fig. 2. We can see that the corrugation of the PES is strongly dependent on the polarity of the sliding paths, whereas the h-BN/h-BN system sliding along path II possesses the largest corrugation [Fig. 2(c)], and the graphene/graphene system the smallest one [Fig. 2(a)]. The magnitude of saddle point interaction energy and the maximum corrugation amplitude of the PES for graphene/graphene and h-BN/h-BN systems can be found in Tables S1 and S2 in the Supplemental Material [29]. To examine the difference of the sliding path on friction, we plotted the potential profiles along the two paths, as indicated

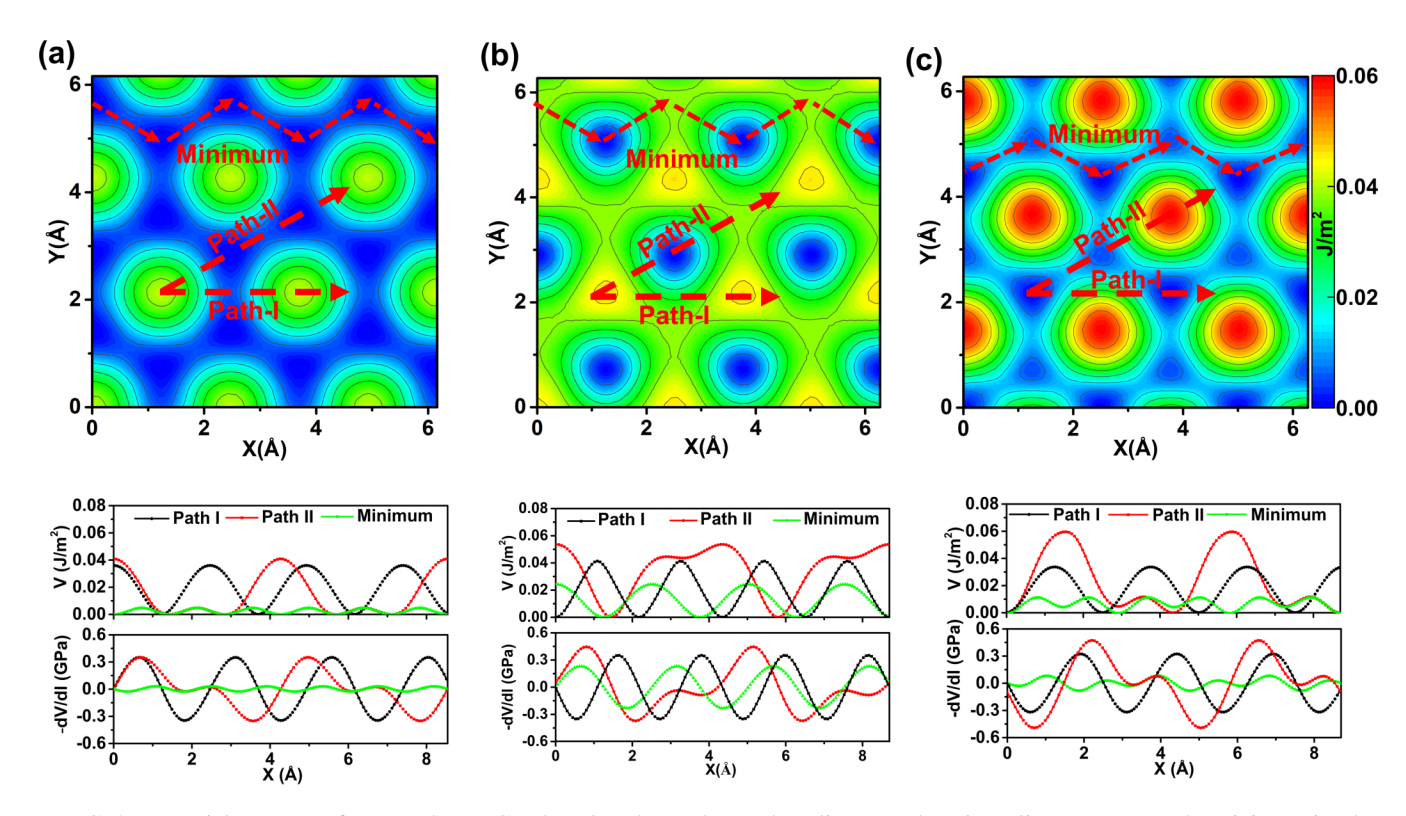


FIG. 2. Potential energy surfaces (PES). (a) Graphene/graphene, (b) graphene/h-BN, and (c) h-BN/h-BN systems. The minimum is taken as a reference. The corresponding potential barrier and friction forces along the three paths are plotted under each PES.

in the middle of Fig. 2. In the graphene/graphene system, of course, they exhibit the same potential energy corrugation. However, for the graphene/h-BN and h-BN/h-BN systems, the corrugation along path II is much larger than that of path I. The lateral forces acting on the slider dragged along the two paths were also calculated and are shown in Fig. 2 (bottom). In all, the anisotropic friction behavior for the polar system [13] is blindingly obvious, which corroborates the results in Fig. 1.

In addition, the majority view is that the real sliding path between neighbor minima at static friction occurs near saddle points of PES. The sliding barrier and friction force along the minimum potential energy path (zigzag path; see Fig. 2 and Fig. S3 in the Supplemental Material [29]) indicate that even for the zigzag path polarity still plays an important role in friction for the *h*-BN/*h*-BN bilayer. We also calculated the PESs for the other two systems, which also exhibit larger friction along the polar path (see Fig. S4 in the Supplemental Material [29]).

From the above calculations, we conclude that the frictional properties exhibited by 2D systems both with and without external load depend on the polarity and hence on the sliding direction. The sliding potential barrier  $\Delta V = \Delta E + F_N \Delta h$ , where  $F_N$  is the external load;  $\Delta E$  and  $\Delta h$  are the changes in the binding energy and the interlayer separation during sliding, respectively [28]. Note that  $\Delta V$  depends on (a) the variation of the adsorption bond energy  $\Delta E$ , and (b) the work done  $F_N \Delta h$  to overcome  $\Delta h$  during sliding. When no external load is applied, the friction is determined by  $\Delta E$ . However, for the normal loads used in our study, the most important contribution to the sliding barrier comes from the

work done against the external force (see Fig. S5 in the Supplemental Material [29]).

The relationship between friction and polarity can be obtained by examining the roughness of charge distribution along different sliding paths. To understand the origin of the anisotropic friction behavior, we calculated the charge density difference of these 2D systems. The charge density difference is calculated by  $\Delta \rho = \rho_{L_1L_2} - \rho_{L_1} - \rho_{L_2}$ , where  $\rho_{L_1L_2}$ ,  $\rho_{L_1}$ , and  $\rho_{L_2}$  are the charge densities of the bilayer layer, top layer  $L_1$ , and bottom layer  $L_2$ , respectively. First, from Figs. 3(a)-3(c) for the graphene/graphene system, the charge distribution between the two graphene layers is uniform and flat along the sliding paths, which corresponds to a small charge corrugation and sliding barrier. Then, for the polar bilayer systems of graphene/h-BN [Figs. 3(d)-3(f)] and h-BN/h-BN [Figs. 3(g)-3(i)], as well as for H-graphene/h-BN and MoS<sub>2</sub>/MoS<sub>2</sub> systems in Fig. S6 in the Supplemental Material [29], along the nonpolar path I, the net positive charge on the upper layer and the negative charge in the bottom layer are uniformly distributed and relatively flat, which also corresponds to a small charge corrugation and sliding barrier. However, along polar path II [Figs. 3(f) and 3(i)], electron-deficient and electron-rich atoms alternately appear in both the bottom and upper layers, which causes a large fluctuation of charge distribution along the sliding direction. Of course, the larger the electronegativity difference, the larger the corrugation of charge distribution and friction. The charge density difference of H-graphene/h-BN and MoS<sub>2</sub>/MoS<sub>2</sub> can be found in Fig. S6 in the Supplemental Material [29].

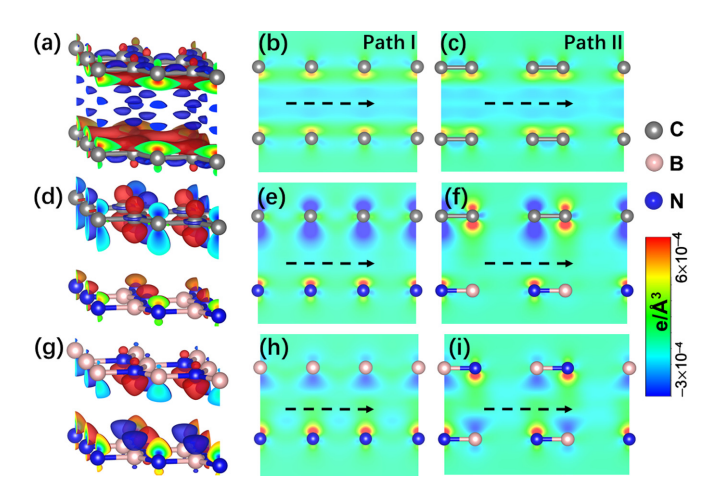


FIG. 3. The charge density difference information. (a) The charge density difference of bilayer graphene, with an isosurface charge density of 0.0003 electrons/Å<sup>3</sup>. The red and blue indicate charge accumulation and depletion regions, respectively, and the dotted arrow lines indicate sliding direction. The corresponding cross-sectional views of the bilayer system along (b) path I and (c) path II. (d)–(f) the case of the graphene/h-BN system and (g)–(i) the case of the h-BN/h-BN system.

To establish a clear relationship between electronegativity difference and interfacial friction, in Fig. 4 we compare the friction properties for all five calculated systems, as shown in Fig. 4(a). The comparisons of COF under the load of  $0.7\,\mathrm{nN/Å^2}$  in different systems shows that along the nonpolar path I, the COFs are almost equal for all the systems, and about  $\sim\!0.1$ , which fall within the range of friction strength dominated by the vdW interaction [5,13,14,40,41]. Note also that the polar path exhibits larger friction than for the nonpolar path for all the systems.

To better understand the different COFs along the polar direction II, we further extracted the functional relation between in-plane charge transfers and shear stress, as shown in Fig. 4(b). As the different charge analysis methods may

yield some deviation, the charge transfers were separately calculated by both the Mulliken and Bader charge analyses. Although the two methods provide a different amount of charge transfers, the change of the charge transfer amount with respect to the friction force is quite similar, with errors falling within a small linear window. Interestingly, a linear functional relationship has been found between averaged frictional forces and the amount of intralayer charge transfer. Compared to the nonpolar path I, the added friction in the polar path II can now be safely attributed to the enhanced charge density corrugation that appears in the polar path.

We define the system's total electronegativity difference along a path as  $\Delta \chi_{\parallel} = |\chi_A - \chi_B| + |\chi_C - \chi_D|$ , where  $\chi_X$  represents the electronegativity of the X atom [see Fig. 1(a)]. By definition, the greater the electronegativity differences between its constituent atoms of each layer, the greater the  $\Delta \chi_{\parallel}$ . Similar to charge transfer in Fig. 4(b), the frictional forces increase with the increase of  $\Delta \chi_{\parallel}$ , which obeys a linear scaling law [Fig. 4(c)].

Finally, to see clearly which type of interactions play the key role on electronegative friction in low-dimensional systems, we further separately calculated the contributions of Coulomb interaction  $V_{\text{Coul}}$  and dispersion force  $V_{\text{disp}}$  to the total sliding energy barrier  $V_{\rm T}$  along two sliding paths, as shown in Fig. 5. First of all, contrary to the traditional belief, instead of the dispersion terms, the Coulomb interaction contributes to most of the sliding potential barrier. For the bilayer graphene system, the Coulomb contributions of the two paths are almost equal [see Figs. 5(a) and 5(b)], but for the bilayer h-BN system, the additional charge distribution induced by polarity enhances the Coulombic contribution to the friction on the polar path, which is almost twice that of the nonpolar path [see Figs. 5(d) and 5(e)]. In addition, we calculated the relationship between the maximum energy barrier  $\Delta V_{\text{max}} = V_{\text{max}} - V_{\text{min}}$ , where  $V_{\text{max}}$  and  $V_{\text{min}}$  are the maximum and minimum of the potential barrier V, and the normal load along the two sliding paths. Interestingly, the sliding barrier from dispersion terms of about 0.01 J/m<sup>2</sup> is in-

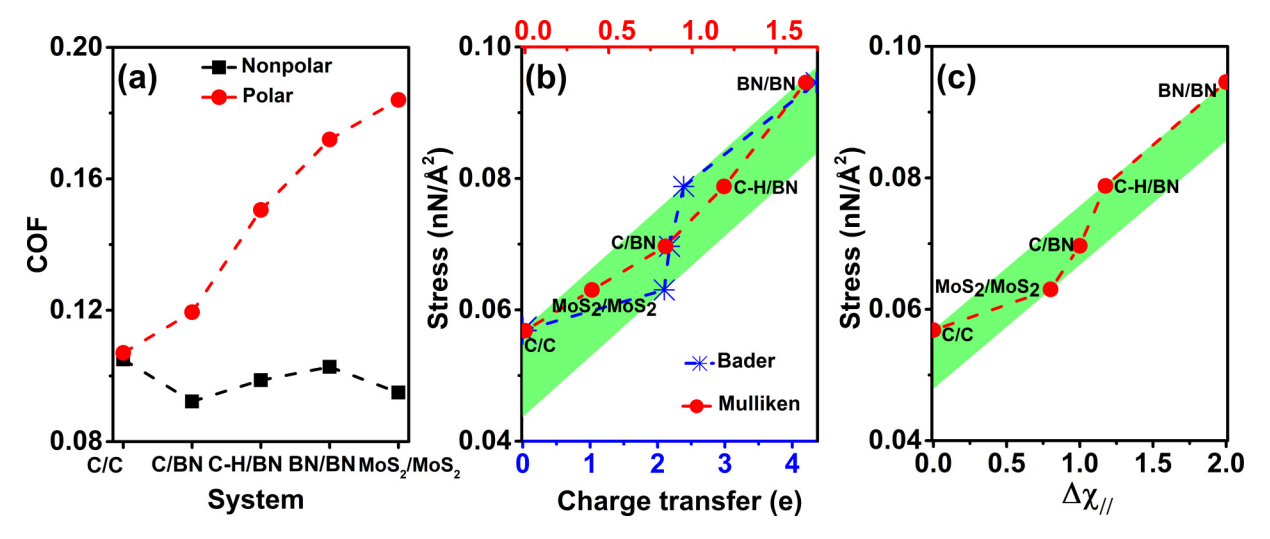


FIG. 4. Linear scaling law of friction. (a) Comparisons of COFs under the load of  $0.7 \, \text{nN/Å}^2$  among different bilayer systems. The shear stress as a function of (b) charge transfer and (c) electronegativity difference  $\Delta \chi_{\parallel}$ .

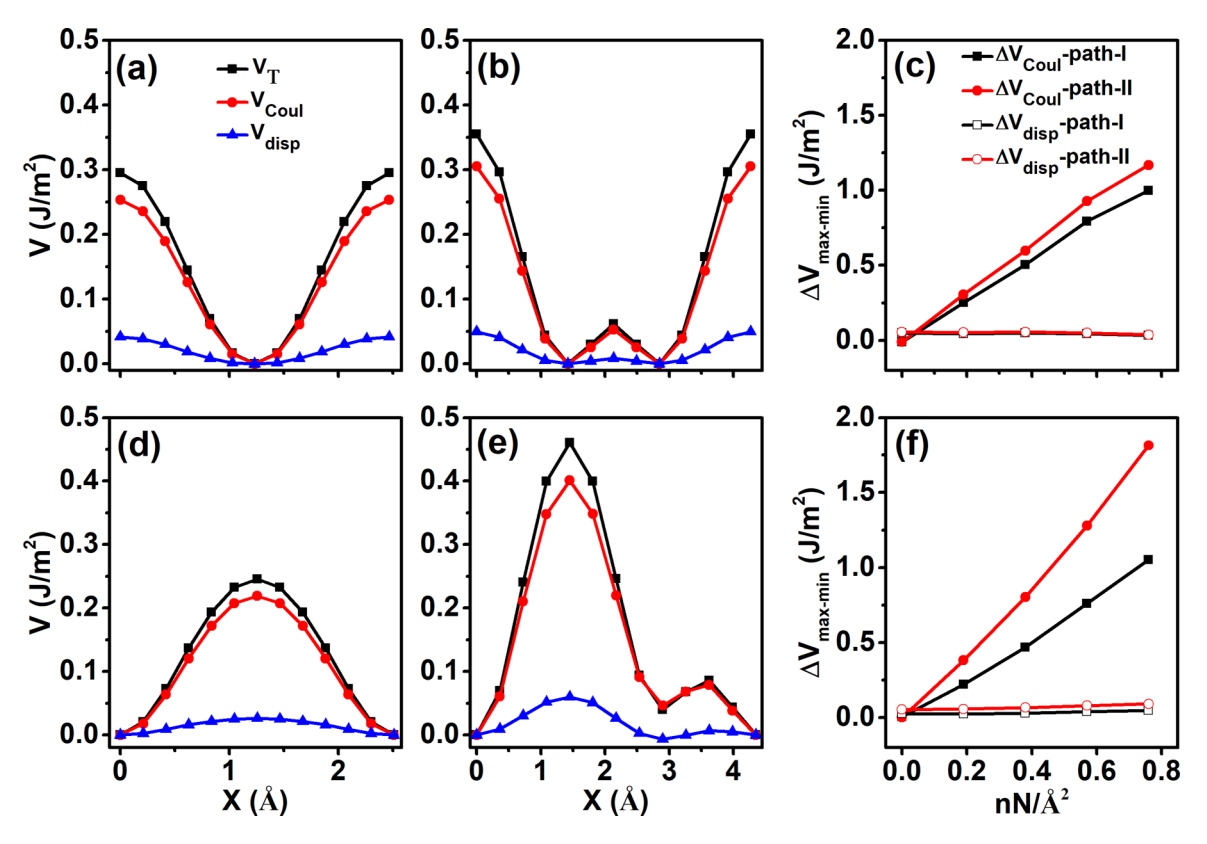


FIG. 5. Components of sliding energy barriers. The contributions of Coulomb interaction  $V_{\text{Coul}}$  and dispersion terms  $V_{\text{disp}}$  to total potential energy  $V_{\text{T}}$  along (a) path I and (b) path II of graphene/graphene, (d) path I, and (e) path II of h-BN/h-BN under the normal load of  $0.2 \, \text{nN/Å}^2$ ; the minimum-energy value along each sliding path is set to 0. The difference of Coulomb interaction and vdW energy between the highest-and lowest-energy stackings as a function of normal load for (c) graphene/graphene and (f) h-BN/h-BN, respectively.

dependent of the external normal load. However, the Coulomb contribution to sliding barrier increases with increasing pressure [see Figs. 5(c) and 5(f)]. Therefore, it can be inferred that the interlayer friction of 2D layered materials is mainly determined by the Coulomb interaction, which is consistent with previous reports [13,42,43]. For nonpolar paths, different 2D vdW materials exhibit similar small Coulomb barriers due to the smooth charge distribution, but for the polar path, the larger the polarity, and the larger charge distribution roughness and Coulomb barrier. The above results provide a full picture for the interlayer friction of 2D systems.

The above analysis shows that the electronegativity difference in one preferred direction dominates the friction behavior along the sliding path for 2D systems. We denote this friction as electronegativity induced friction, which obeys a linear scaling law. It should be emphasized here that all the sliding interfaces in our calculation are commensurate. For elastically stiff 2D layers the polarity effect will be canceled for the incommensurate interface, such as identical double layers with relative rotation. However, if the effective elastic modulus is low enough commensuratelike domains may form, and the discussion above is relevant for these cases too.

In our previous studies, we proposed the charge roughness mechanism of nanofriction [8]. By comparing the tribological properties of graphene and hydrogenated graphene, we found that the coefficient of friction is proportional to the roughness of the charge distribution of the interface. In present work, we further show that the friction of the system is directly related

to the corrugation of charge distribution in the sliding path by comparing the friction of different 2D systems. In polar systems, the electronegativity differences between component atoms can induce additional charge roughness, increasing the friction of the system.

# IV. CONCLUSION

Using the DFT with dispersion correction, the role of electronegativity in interfacial friction has been investigated. We have shown that these 2D systems exhibit almost the same friction along a nonpolar sliding path as the similar uniform charge distribution. In contrast, the interfacial friction force along the polar path is proportional to the electronegativity difference among its constituent atoms. This linear scaling relationship between friction and electronegativity difference can be extended to other low-dimensional materials such as multiwall nanotubes and nanosheets [11], which will provide not only an alternative perspective in the field of tribology, but also a strategy for controlling friction at the nanoscale.

### ACKNOWLEDGMENT

The work was supported by the National Natural Science Foundation of China (Grants No. U1604131, No. 11774078, and No. 11805295).

The authors declare no competing interests.

- [1] M. Urbakh and E. Meyer, Nat. Mater. 9, 8 (2010).
- [2] O. M. Braun and A. G. Naumovets, Surf. Sci. Rep. **60**, 79 (2006).
- [3] C. Lee, Q. Li, W. Kalb, X. Liu, H. Berger, R. W. Carpick, and J. Hone, Science 328, 76 (2010).
- [4] J. C. Spear, B. W. Ewers, and J. D. Batteas, Nano Today 10, 301 (2015).
- [5] S. Cahangirov, C. Ataca, M. Topsakal, H. Sahin, and S. Ciraci, Phys. Rev. Lett. 108, 126103 (2012).
- [6] O. Hod, E. Meyer, Q. Zheng, and M. Urbakh, Nature (London) 563, 485 (2018).
- [7] R. C. Sinclair, J. L. Suter, and P. V. Coveney, Adv. Mater. 30, 1705791 (2018).
- [8] J. Wang, J. Li, L. Fang, Q. Sun, and Y. Jia, Tribol. Lett. 55, 405 (2014).
- [9] M. Wolloch, G. Levita, P. Restuccia, and M. C. Righi, Phys. Rev. Lett. 121, 026804 (2018).
- [10] B. Wolter, Y. Yoshida, A. Kubetzka, S.-W. Hla, K. von Bergmann, and R. Wiesendanger, Phys. Rev. Lett. 109, 116102 (2012).
- [11] A. Niguès, A. Siria, P. Vincent, P. Poncharal, and L. Bocquet, Nat. Mater. 13, 688 (2014).
- [12] G. Tocci, L. Joly, and A. Michaelides, Nano Lett. 14, 6872 (2014).
- [13] N. Marom, J. Bernstein, J. Garel, A. Tkatchenko, E. Joselevich, L. Kronik, and O. Hod, Phys. Rev. Lett. 105, 046801 (2010).
- [14] O. Hod, J. Chem. Theory Comput. 8, 1360 (2012).
- [15] W. Gao and A. Tkatchenko, Phys. Rev. Lett. 114, 096101 (2015).
- [16] G. Kresse and J. Furthmüller, Phys. Rev. B 54, 11169 (1996).
- [17] G. Kresse and D. Joubert, Phys. Rev. B **59**, 1758 (1999).
- [18] P. E. Blöchl, Phys. Rev. B 50, 17953 (1994).
- [19] J. P. Perdew, K. Burke, and M. Ernzerhof, Phys. Rev. Lett. 77, 3865 (1996).
- [20] A. Tkatchenko, R. A. DiStasio, R. Car, and M. Scheffler, Phys. Rev. Lett. 108, 236402 (2012).
- [21] H. J. Monkhorst and J. D. Pack, Phys. Rev. B 13, 5188 (1976).
- [22] G. Constantinescu, A. Kuc, and T. Heine, Phys. Rev. Lett. 111, 036104 (2013).
- [23] P. E. Sheehan and C. M. Lieber, Science 272, 1158 (1996).
- [24] S. G. Balakrishna, A. S. de Wijn, and R. Bennewitz, Phys. Rev. B 89, 245440 (2014).

- [25] W. Wang, J. Shen, and Q.-C. He, Phys. Rev. B 99, 054103 (2019).
- [26] D. J. Diestler, E. Rajasekaran, and X. C. Zeng, J. Phys. Chem. B 101, 4992 (2007).
- [27] M. R. Vazirisereshk, H. Ye, Z. Ye, A. Otero-de-la-Roza, M.-Q. Zhao, Z. Gao, A. T. C. Johnson, E. R. Johnson, R. W. Carpick, and A. Martini, Nano Lett. 19, 5496 (2019).
- [28] W. Zhong and D. Tománek, Phys. Rev. Lett. 64, 3054 (1990).
- [29] See Supplemental Material at http://link.aps.org/supplemental/ 10.1103/PhysRevB.105.165431 for detailed energies of symmetric stackings of graphene/graphene and h-BN/h-BN systems, friction comparison between graphene/graphene and graphene/h-BN systems along minimum potential energy paths, sliding models, potential energy surface (PES), and charge density difference for H-graphene/h-BN and MoS<sub>2</sub>/MoS<sub>2</sub> systems, which includes Refs. [15,30–36].
- [30] J. He, K. Hummer, and C. Franchini, Phys. Rev. B 89, 075409 (2014).
- [31] M. Wen, S. Carr, S. Fang, E. Kaxiras, and E. B. Tadmor, Phys. Rev. B 98, 235404 (2018).
- [32] I. V. Lebedeva, A. V. Lebedev, A. M. Popov, and A. A. Knizhnik, Comput. Mater. Sci. 128, 45 (2017).
- [33] A. M. Popov, I. V. Lebedeva, A. A. Knizhnik, Y. E. Lozovik, and B. V. Potapkin, Chem. Phys. Lett. 536, 82 (2012).
- [34] P. H. Tan, W. P. Han, W. J. Zhao, Z. H. Wu, K. Chang, H. Wang, Y. F. Wang, N. Bonini, N. Marzari, N. Pugno, G. Savini, A. Lombardo, and A. C. Ferrari, Nat. Mater. 11, 294 (2012).
- [35] Y. Baskin and L. Meyer, Phys. Rev. 100, 544 (1955).
- [36] R. Zacharia, H. Ulbricht, and T. Hertel, Phys. Rev. B 69, 155406 (2004).
- [37] J. H. Warner, M. H. Rümmeli, A. Bachmatiuk, and B. Büchner, ACS Nano 4, 1299 (2010).
- [38] B. N. J. Persson, Tribol. Lett. 68, 28 (2020).
- [39] G. Zilibotti and M. C. Righi, Langmuir 27, 6862 (2011).
- [40] S. Zhou, J. Han, S. Dai, J. Sun, and D. J. Srolovitz, Phys. Rev. B 92, 155438 (2015).
- [41] B. Li, J. Yin, X. Liu, H. Wu, J. Li, X. Li, and W. Guo, Nat. Nanotechnol. 14, 567 (2019).
- [42] M. Reguzzoni, A. Fasolino, E. Molinari, and M. C. Righi, Phys. Rev. B 86, 245434 (2012).
- [43] O. V. Ershova, T. C. Lillestolen, and E. Bichoutskaia, Phys. Chem. Chem. Phys. 12, 6483 (2010).